Applied Energy 212 (2018) 478–488

Contents lists available at ScienceDirect

Applied Energy

journal homepage: www.elsevier.com/locate/apenergy

Exploration of the material property space for chemical looping air separation applied to carbon capture and storage

R.H. Görke[a], W. Hu[a,b], M.T. Dunstan[c], J.S. Dennis[d], S.A. Scott[a,*]

[a] Department of Engineering, University of Cambridge, Trumpington Street, Cambridge CB2 1PZ, United Kingdom
[b] School of Engineering, Newcastle University, Merz Court, Newcastle upon Tyne NE1 7RU, United Kingdom
[c] Department of Chemistry, University of Cambridge, Lensfield Road, Cambridge CB2 1EW, United Kingdom
[d] Department of Chemical Engineering and Biotechnology, University of Cambridge, Pembroke Street, Cambridge CB2 3RA, United Kingdom

HIGHLIGHTS

- Coupling material properties to a steady-state oxy-fuel power plant model.
- A map to estimate *a priori* the performance and viability of redox materials.
- Screening of 2857 candidate materials using large databases of material properties.
- Energy penalty of carbon capture found to be as low as 1.5 percentage points.

ARTICLE INFO

Keywords:
Carbon capture and storage
Air separation
Chemical looping
Oxygen carrier
Oxygen production

ABSTRACT

Oxy-fuel combustion is one route to large scale carbon capture and storage. Fuel is combusted in oxygen rather than air, allowing pure CO_2 to be captured and sequestered. Currently, the required oxygen is produced *via* cryogenic air separation, which imposes a significant energy penalty. Chemical looping air separation (CLAS) is an alternative process for the production of oxygen, and relies on the repeated oxidation and reduction of solid oxygen carriers (typically metal oxides). The energy efficiency is governed by the thermodynamic properties of the oxygen carrier material, and how well the CLAS process can be heat-integrated with the process consuming oxygen. In this study, key thermodynamic properties have been identified and assessed using a steady state model of a CLAS-oxy-fuel power plant. It is demonstrated that energy penalties as low as 1.5 percentage points can be obtained for a narrow range of material properties. Based on density functional theory calculations, 14 oxygen carrier systems, which are novel or have received little attention, have been identified that could potentially achieve this minimal energy penalty.

1. Introduction

The oxy-fuel process is a promising approach for capturing carbon dioxide from power plants fired with fossil fuels [1]. Here, fossil fuels are burnt in a mixture of CO_2 and O_2, ultimately yielding a stream of CO_2 sufficiently pure for sequestration in geological formations [2]. The cost of the energy required to produce the oxygen needed for combustion is currently a major drawback. Using cryogenic air separation to supply pure oxygen results in a reduction in the net efficiency of a typical power plant of ca. 8–10 percentage points [3–5].

A potential way to overcome this energy penalty is to exploit a technique commonly referred to as chemical looping to separate oxygen from the air. A chemical looping process is characterized by the cyclic reduction and oxidation of solid material, termed here the *oxygen carrier*. The commercial production of oxygen using such a scheme dates back to 1880 when it was successfully realized by Arthur and León Brin [6]. However, one of the drawbacks of the Brin process, which looped between BaO and the peroxide BaO_2, was the need to first remove the carbon dioxide present in the air, which otherwise led to the irreversible formation of $BaCO_3$. Consequently, the Brin process was superseded by the cryogenic separation of air in the early 20th century. In 2000, the idea of exploiting a chemical loop for the separation of air was reintroduced, in this case using a perovskite (LSCF) as the oxygen carrier [7,8]. Later, simpler compounds, such as CuO/Cu_2O, Mn_2O_3/Mn_3O_4 and CoO/Co_3O_4, were considered as oxygen carriers [9,10]. At high temperatures, copper oxide and other transition metal oxides do not react with the CO_2 in air to form stable carbonates under process conditions.

* Corresponding author.
E-mail address: sas37@cam.ac.uk (S.A. Scott).

https://doi.org/10.1016/j.apenergy.2017.11.083
Received 18 July 2017; Received in revised form 26 October 2017; Accepted 18 November 2017
Available online 22 December 2017

Nomenclature

CLAS	chemical looping air separation
DFT	density functional theory
HRSG	heat recovery steam generator
LHV	lower heating value
LSCF	lanthanum strontium cobalt ferrite
OC	oxygen carrier
$\Delta C_{p,r}$	molar heat capacity of reaction (J/K/mol)
ΔG_r^o	Gibbs free energy of reaction at 1 bar (J/mol)
ΔH_r^o	enthalpy of reaction at 1 bar (kJ/mol)
ΔS_r^o	entropy of reaction at 1 bar (J/K/mol)
ΔT_{min}	minimum temperature difference in heat exchanger (K)
ΔT_r	temperature difference between oxidizer and reducer (K)
$\dot{N}_{solid}$	solids circulation between the oxidizer and reducer (mol/s)
$\dot{N}_{CO_2}$	flow of carbon dioxide from the reducer (mol/s)
$\dot{N}_{H_2O}$	flow of water separated out in the CLAS condenser (mol/s)
$\dot{N}_{O_2,ox,in}$	flow of oxygen to the oxidizer (mol/s)
$\dot{N}_{O_2,red}$	flow of oxygen from the reducer (mol/s)
$\dot{N}_{solid}$	flow of steam from the reducer (mol/s)
P_{O_2}	equilibrium partial pressure of oxygen (bar)
$P_{O_2,air}$	oxygen partial pressure of air (bar)
$P_{O_2,ox}$	operating partial pressure of oxygen of the oxidizing reactor (bar)
$P_{O_2,red}$	operating partial pressure of oxygen of the reducing reactor (bar)
$P_{O_2,req}$	partial pressure of oxygen required by the oxy-fuel combustor (bar)
P_{tot}	operating pressure of the reducer (bar)
$\dot{Q}$	heat flow between the oxidizer and reducer (W)
R	universal gas constant (J/K/mol)
RH	relative humidity (%)
$S_{O_2}^o$	entropy of formation of oxygen at 1 bar (J/K/mol)
T	temperature (K)
T_{dew}	dew point temperature (K)
T_{eq}	equilibrium temperature of the oxygen carrier with oxygen and operating temperature of the reducer (K)
y_i	mole fraction of species i in the gas phase (–)
α	ratio of activities of the solids
μ	chemical potential (J/mol)
χ_{inert}	molar fraction of inert material in the solid phase (–)

A putative process flow diagram for a CLAS-oxy-fuel power plant is shown in Fig. 1. The power plant can be subdivided into three parts: (i) the chemical looping air separation (CLAS) unit, (ii) combustion of the fuel including carbon sequestration, and (iii) a steam cycle for power generation. The flue gas leaving the oxy-fuel combustor will require cleaning to remove particulate matter and sulphurous gases, derived from the fuel. The CLAS unit would consist of two interconnected fluidized beds, *viz.* the oxidizer and reducer [10]. By cycling the oxygen carrier between the oxidizer and reducer, continuous oxygen production can be achieved in the latter. If an existing power plant were to be retrofitted for oxy-fuel combustion, the composition of the incoming oxidizing gas would have to allow the combustor to operate within its envelope of design parameters (*e.g.* to ensure a correct heat transfer coefficient) [11–13]. Accordingly, an oxy-fuel combustor would typically require a mole fraction of oxygen of around 0.3–0.35, with the balance being CO_2 when a dry recycle is used (oxy-dry combustion) [11,12]. The condenser in Fig. 1 allows the mass fraction of oxygen entering the combustor to be altered, by allowing for the removal of water, which may have been injected into the reducer as steam.

The selection and identification of suitable oxygen carrier materials is crucial to the feasibility of a CLAS process. Oxygen carriers must operate at intermediate to high temperatures for a long period of time

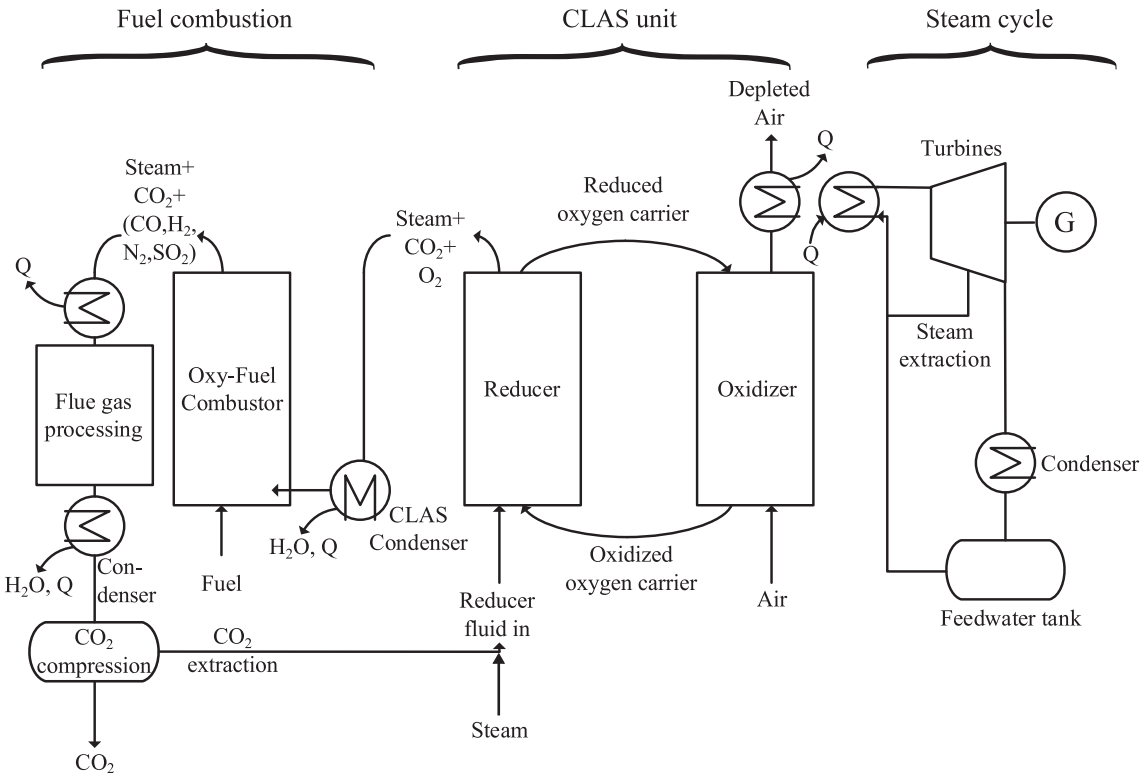

Fig. 1. Flow diagram of a proposed CLAS-oxy-fuel power plant. Q denotes a heat source or sink as indicated by the arrows.

to give economic production of oxygen. Three different types of oxygen carriers have been identified for use in more general chemical looping processes, *e.g.* chemical looping combustion: single metal oxides [14–17]; composite metal oxides [16–19]; and perovskite-type oxides [16,17,20–22]. In the listed order, the oxygen transfer capacity per unit mass of the carrier generally decreases and the mechanical strength and cost of material generally increases. In chemical looping systems, a material combining both a high oxygen transfer capacity and rapid rates of reaction for both oxidation and reduction is desirable because this gives the lowest rate of circulation between the reactors. To minimize operating expenditure, the oxygen carrier material should exhibit high mechanical strength and chemical stability to prevent too frequent a replenishment of the depleted carrier with fresh material. The work here is focused on the thermodynamic properties of the oxygen carrier. Whilst other criteria, such as mechanical strength or high reaction rates, are important, the thermodynamics of the oxygen release reaction,

$$XO_2 \rightleftarrows X + O_2$$

determine, to a large extent, the feasibility of the CLAS process. In particular, the equilibrium partial pressure (P_{O_2}) for this reaction as a function of temperature determines possible operating regimes, and is related to the Gibbs free energy of reaction, ΔG_r^o by

$$P_{O_2} = \exp\left(-\frac{\Delta G_r^o}{RT}\right)\alpha \tag{1}$$

where the ratio of the activities of the solids, α, is usually taken as unity [17].

2. Methodology

In previous studies, materials that are thought to perform well as oxygen carriers were selected first and only subsequently assessed. In contrast, the inverse design approach is a method that identifies the desired material properties required by the process first, followed by the identification of materials possessing such properties using first-principles computations, such as calculations using density functional theory (DFT). This approach has been successfully executed for the identification of unreported and thermodynamically-stable ternary materials [23–25]. Here, the inverse design approach has been applied to identify functional oxygen carrier materials for CLAS. The strategy involves constructing a full (steady state) model of a CLAS system integrated with an oxy-fuel power station. This model assumes the availability of a generic oxygen carrier material with an arbitrary set of characteristic thermodynamic properties. Searching the space of thermodynamic properties of the generic material then allows desirable characteristics to be identified and compared with known or computed oxide materials.

2.1. CLAS integration with a steam power plant

In this study, the energy penalty imposed by flue gas processing and carbon dioxide compression was neglected, because these processes present an equal decrease in efficiency for all oxy-fuel power plants. The reducing reactor has to be fluidized by a gas with a low partial pressure of oxygen. Here, this can be either recycled CO_2 with or without injected steam. In the model, the steam needed could either be provided by the steam cycle, *e.g.* from the low-pressure turbine, or by using other sources of heat to evaporate water.

Here, the oxy-fuel combustor requires a fluidizing gas containing a mole fraction of oxygen of roughly 0.35 at ambient pressure when operating with a dry recycle, *i.e.* when almost no steam is present in the gas. This should then give a rate of heat transfer between the gases leaving the combustor and boiler tubes comparable to that when combusting with air [12]. The CLAS condenser shown in Fig. 1, allows the partial pressure of oxygen to be increased to the desired level by condensing injected steam. Assuming that steam can be bled from, or introduced into, the low-pressure turbine, and water can be withdrawn from, or introduced into, the feedwater tank, then evaporation of the water condensed in the CLAS condenser and its reintroduction into the low-pressure turbine would close the steam cycle. Further, the partial pressure of oxygen required by the combustor, $P_{O_2,req}$, and the operating partial pressure of oxygen of the reducing reactor, $P_{O_2,red}$, dictate the amount of steam required in the reducer:

$$P_{O_2,red} = \frac{\dot{N}_{O_2,red}}{\dot{N}_{steam} + \dot{N}_{CO_2} + \dot{N}_{O_2,red}} \times P_{tot} \tag{2}$$

$$P_{O_2,req} \equiv 0.35 \times P_{tot} = \frac{\dot{N}_{O_2,red}}{\dot{N}_{steam} + \dot{N}_{CO_2} + \dot{N}_{O_2,red} - \dot{N}_{H_2O}} \times P_{tot} \tag{3}$$

where P_{tot} is the operating pressure of the reducer, $\dot{N}_{O_2,red}$, $\dot{N}_{steam}$ and $\dot{N}_{CO_2}$ are the molar flow of oxygen, steam and carbon dioxide from the reducer. $\dot{N}_{H_2O}$ is the molar flow of water separated out in the CLAS condenser, which can be determined by performing a dew point calculation given by

$$T_{dew} = \frac{243.12a_1}{17.62 - a_1} - 273.15 \tag{4}$$

$$a_1 = \frac{\ln RH + 17.62(T - 273.15)}{T - 30.03} \tag{5}$$

where RH is the relative humidity and T the temperature (K) [26].

Each reactor in Fig. 1, *viz.* the oxidizing and reducing reactors of the CLAS dual fluidized bed and the oxy-fuel combustor, was modelled as being well mixed with respect to both gas and solid phases, and assuming thermodynamic equilibrium between the exit streams.

2.2. Thermodynamics

Assuming equilibrium, the oxygen released by the oxygen carrier in the reducing reactor of the CLAS unit depends solely on the equilibrium partial pressure of oxygen of the material's oxygen release reaction, which in turn depends on ΔG_r^o according to Eq. (1). It follows from

$$\Delta G_r^o = \Delta H_r^o - T\Delta S_r^o \tag{6}$$

that the Gibbs free energy of reaction is a function of the enthalpy of reaction, ΔH_r^o, the temperature, T, and the entropy of reaction, ΔS_r^o.

Using the van't Hoff equation

$$\frac{\partial}{\partial T}\left(\frac{\Delta G_r^o}{T}\right) = -\frac{\Delta H_r^o}{T^2} \tag{7}$$

the Gibbs free energy of reaction can be rewritten as a function of the enthalpy of reaction, ΔH_r^o, and temperature only, where

$$\Delta H_r^o(T_2) = \Delta H_r^o(T_1) + \int_{T_1}^{T_2} \Delta C_{p,r}\, dT \tag{8}$$

The Gibbs free energy of reaction at temperature T_1 and T_2 are then related by

$$\frac{\Delta G_r^o(T_2)}{T_2} - \frac{\Delta G_r^o(T_1)}{T_1} = -\int_{T_1}^{T_2} \frac{\Delta H_r^o(T)}{T^2} dT = \Delta H_r^o(T_1)\left(\frac{1}{T_2} - \frac{1}{T_1}\right) - \int_{T_1}^{T_2} \frac{\int_{T_1}^{T} \Delta C_{p,r}(T')dT'}{T^2} dT \tag{9}$$

In subsequent calculations, it was assumed that the solids obey the Dulong-Petit law, so that the molar heat capacity of reaction, $\Delta C_{p,r}$, is linked to the molar heat capacity of the oxygen released, $C_{p,O_2}(T)$, by

$$\Delta C_{p,r}(T) = \nu_{O_2}(C_{p,O_2}(T) - 6R) \tag{10}$$

where ν_{O_2} denotes the stoichiometric coefficient of oxygen in the reduction reaction; here, the stoichiometric coefficient of oxygen is set to 1. Accordingly, the enthalpy of reaction, $\Delta H_r^o(T_{eq})$ at the temperature of the reducing reacting reactor (T_{eq}) can then be linked, using Eq. (1), to

the equilibrium partial pressure of oxygen in the reducing reactor and the temperature of oxidizing reactor (which is constrained to operate with a partial pressure below 0.21 bar) by

$$Rln\left(\frac{P_{O2,red}}{P_{O2,ox}}\right) = \Delta H_r^o(T_{eq})\left(\frac{1}{T_{ox}} - \frac{1}{T_{eq}}\right) + F(T_{ox},T_{eq}) \quad (11)$$

If the temperature difference between the oxidizer and the reducer is fixed (here to 80 K), the effect of the material on the system is therefore determined by three parameters, $\Delta H_r^o(T_{eq})$, T_{eq}, and the reaction stoichiometry, given a desired value of $P_{O2,red}$. There is a minor contribution from the term $F(T_{ox},T_{eq})$, which arises from the change in heat capacity for the reaction, *i.e.* the inner integral of Eq. (9), and can largely be ignored. Here, $F(T_{ox},T_{eq})$ is retained simply to ensure consistency in the calculations. Whilst the heat capacities of the solids have little effect on the equilibrium partial pressure, they do have a large effect on the heat balance, since they determine how much heat is circulated between the reducer and the oxidizer.

The mass and energy balances for the CLAS oxy-fuel system were computed in MATLAB; all thermodynamic (*i.e.* enthalpy, entropy and free energy) data for the non-fictitious species were taken from the NASA Glenn database [27]. For the fictitious materials and those derived from density functional theory (DFT), since only the differences in enthalpy and entropy between reduced and oxidized states are important, the values for the reduced phase were set arbitrarily and the oxidized phases set relative to that. In addition, for the entropy, it was assumed the production of gaseous oxygen dominates the entropy of reaction at 298 K, *i.e.* $\Delta S_r^o(298K) \equiv S_{O_2}^o(298\ \mathrm{K})$ [25]. The values of the molar heat capacity, C_p, for the oxidized and reduced phases were set using the Dulong-Petit law.

Subject to constraints to ensure conservation of atoms, the equilibrium was found by minimizing the total Gibbs energy, $G_T = \sum \mu(i)N_i$, using the optimization toolbox of MATLAB. For solids, the chemical potential is equal to the standard molar Gibbs free energy of formation, as shown in Eq. (12). The standard Gibbs free energy is determined using Eq. (13).

$$\mu_{solid}(i) = G_i^o \quad (12)$$

$$G_i^o = H_i^o - TS_i^o \quad (13)$$

For gases, which are assumed to be ideal in this case, a term taking into account mixing effects must be included, leading to

$$\mu_{gas}(i) = G_i^o + (RT)\left(\ln\frac{P_{tot}}{P_0} + \ln y_i\right) \quad (14)$$

where T is the temperature, P_{tot} is the total pressure, y_i is the mole fraction of species i in the gas phase. The outlet of the oxy-fuel combustor was constrained to contain 1% of the initial carbon as unburned coal. From the heat released, composite curves were generated for heat integration analysis. The CLAS dual fluidized bed reactor was fully heat integrated with the oxy-fuel combustor and then both were scaled to match the heat demand of a steam cycle for a specific gross power output; in this case 500 MW_{el}. The reference steam cycle was based on unit 5 of the Großkrotzenburg Power Station, Germany, and is characterized by electricity generated at 1.31 MW/kg of steam and a specific heat demand of the steam as shown in Fig. 2 [28,29]. It should be noted that the specific electricity generation involves only the heat demand of the heat recovery steam generator (HRSG). The maximum steam cycle temperature, which is an important parameter for the heat integration and overall process efficiency, is 835 K. In this model, the properties of the steam around the steam cycle were calculated using the IAPWS IF-97 method (XSteam) [30]. The net efficiency of the base steam cycle was calculated to be 42.1%. Deviations from 42.1% are possible when the operating temperature of the oxidizer falls below the maximum steam cycle temperature, *i.e.* the highest turbine inlet temperature; in this case, heat integration is not possible without modifying the turbines in the steam cycle. A detailed description of the modifications made to the flow sheet to accommodate these lower turbine inlet temperatures is given in the supplementary information.

2.3. Oxygen carrier materials

The redox reaction for the oxygen carrier systems was assumed to follow

$$4XO \rightleftarrows 2X_2\ O + O_2$$

where X may resemble any combination of elements, metallic or non-metallic, as long as the reaction stoichiometry is maintained, *e.g.* $4CuO \rightleftarrows 2Cu_2\ O + O_2$. The main effect of altering the number of atoms in X is to alter the rate at which heat is transferred between the reducer and oxidizer (*via* changes in the heat capacity). For the fictitious materials, in the base case, the stoichiometry for copper oxide decomposition is assumed for the purposes of setting the solid heat capacities, however other cases are considered in the supplementary information.

Fictitious oxygen carriers were assessed on the basis of a parameter sweep. The sweep was performed for the enthalpy of reaction, $\Delta H_r^o(T_{eq})$, and the equilibrium temperature, T_{eq}, at a fixed $P_{O2,red}$. With the desired $P_{O2,red}$ set, the rate of flue gas re-circulation (and solid oxide circulation) are then determined to give full conversion of the oxygen carrier in the reducer. From Eq. (9) it becomes apparent that specifying ΔH_r^o, T_{eq}, $P_{O2,red}$, and the temperature difference between the oxidizer determines the entropy of reaction, ΔS_r^o. Therefore, in the parameter sweep

$$\left\{100\frac{\mathrm{kJ}}{\mathrm{mol}} \leqslant \Delta H_r^o(T_{eq}) \leqslant 400\frac{\mathrm{kJ}}{\mathrm{mol}}\right\}$$

$$\{773\ \mathrm{K} \leqslant T_{eq} \leqslant 1173\ \mathrm{K}\}$$

the entropy of reaction, ΔS_r^o, is a function of $\{\Delta H_r^o, T_{eq}\}$. Hence, for the parameter sweep, the lower and upper limit of ΔS_r^o is 94.2 J/K/mol and 526.4 J/K/mol, respectively.

$P_{O2,red}$ is limited by the requirement of the oxy-fuel combustor to have an inlet partial pressure of oxygen, $P_{O2,req}$, of roughly 0.35 bar. In the base case, $P_{O2,red}$ was set to 0.34 bar so that the typical oxygen concentration entering the combustor was ~0.35 bar once a fraction of water in the stream was removed by the CLAS condenser; *i.e.* the actual P_{O_2} entering the combustor varied slightly between cases. The outlet temperature of the CLAS condenser was assumed to be 298 K. This base case has no additional steam input into the CLAS reducer, other than that carried around with the wet flue gas. Fig. S1 in the supplementary information shows the case for $P_{O2,red} = 0.2$ bar whilst maintaining a

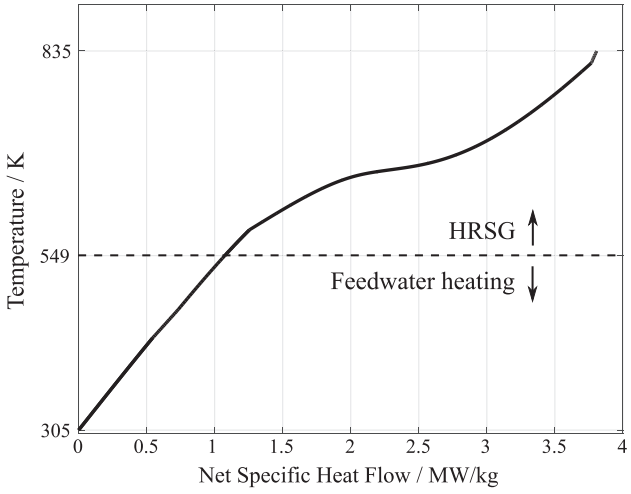

Fig. 2. Specific heat demand of the underlying steam cycle; HRSG: Heat recovery steam generator.

partial pressure of oxygen at the combustor entrance of about 0.35 bar, by injecting additional steam into the CLAS reducer.

Except for the fictitious oxygen carrier materials, the underlying thermodynamic data were taken from the NASA Glenn database [27], NIST-JANAF [31] and Barin and Knacke's [32] tables, if such data existed (here CuO/Cu_2O, Mn_2O_3/Mn_3O_4 and CoO/Co_3O_4). Otherwise the enthalpies of reaction at standard state for various materials were computed based on density functional theory calculations from the Materials Project [33,34]. Additional corrections to account for temperature effects and optimal Hubbard U values for transition elements were employed as described in previous studies [35,36]. The assumptions made for materials taken from the Materials Project regarding the entropy of reaction and the temperature dependence of the thermodynamic properties were the same as for the fictitious materials.

2.4. Fuels

Three different solid fuels, a lignite (Hambach lignite) and two bituminous coals (Illinois No. 5 and Taldinskaya), were considered as well as methane [37]. The ultimate analysis, and heating values of the solid fuels are shown in Table S1 in the supplementary information. The composition of the exhaust gas of the oxy-fuel combustor as well as the rate of circulation of the oxygen carrier in the CLAS unit are dependent on the fuel used. The amount of oxygen supplied is 5% above that required stoichiometrically to achieve complete combustion [13].

3. Determination of optimal steam flow to reducer

As shown below, in many cases the steam cycle is poorly matched to the characteristics of the oxygen carrier. Often heat remains unused at temperatures below the entrance temperature of the HRSG, *viz.* 549 K. This surplus heat was assumed to generate extra steam which was introduced into the low-pressure turbine to produce additional electricity. Similarly, additional steam is bled from the low-pressure turbine if the requirement for steam exceeds the amount of steam that could be produced efficiently. This means that the steam required by the reducer is met partially by evaporation of water from available heat and partially by extracting extra steam from the steam turbine. This leads to a modification of the underlying flow sheet and changes the amount of electricity generated per kg of steam.

Three different cases were identified:

- Case 1: insufficient heat supplied to the reducer, *viz*. the heat demand of the oxygen production is higher than the heat supplied by the combustion of fuel.
- Case 2A: autothermal operation, and
- Case 2B: autothermal operation with significantly decreased efficiencies (i.e. higher energy penalties).

3.1. Case 1: Insufficient heat supplied to the reducer

In this case, the oxy-fuel combustor does not provide sufficient heat to drive the reducer. This can be seen in Fig. 3, which shows the grand composite curve of a CLAS-oxy-fuel power plant producing 500 MW_{el}; in both cases shown in the figure, the combined CLAS unit + the oxy-fuel combustor are scaled to match the heat demand of the steam cycle. In Fig. 3a, the CLAS unit is sized to produce enough oxygen to combust the fuel (with 5% excess). The grand composite curve in Fig. 3a shows that, with this particular material, producing all the oxygen by CLAS is not feasible; the heat provided by the oxy-fuel combustor is insufficient to match the demands of the reducer. In the case shown, using an oxygen carrier with T_{eq} ($P_{O_2,red}$ = 0.34 bar) of 973 K and ΔH_r^o of 250 kJ/mol with Illinois No. 5 coal results in a deficit in heat of 10.3%. Therefore, either heat or additional oxygen must come from elsewhere.

Fig. 3b shows the same plant with a scaled-up oxy-fuel combustor to cover the unmatched heat demand (but keeping the CLAS heat demands constant). Of course, this requires extra oxygen to be provided from elsewhere, with an accompanying energy penalty. For modern cryogenic air separation units (CASU), this penalty is as low as 0.16 kWh per kg of O_2, assuming a CASU plant size of 5000 t per day and a purity of 95% O_2 [38]. In the case of an CLAS-oxy-fuel power plant, it should be noted that the energy penalty might be larger owing the demand for oxygen being much lower than 5000 t per day (*i.e.* ~600 t per day). In practice, because of economies of scale, cryogenic air separation would not complement CLAS and is more likely to substitute it.

Fig. 3a also illustrates that at low temperatures, heat is rejected (Q_2) which could be used to raise steam. Here, this additional heat is utilized by generating additional steam at 427 K, which is then introduced into the low-pressure turbine to generate additional electricity; thus, optimizing the efficiency of the plant. This additional heat sink has been included Fig. 3b, and is included in all subsequent calculations. In this case, this raises the overall efficiency to 41.3% from 38.5% because of the additional production of 66.9 kg/s of steam.

3.2. Case 2: Autothermal operation

For some CLAS materials, it is possible to produce all the oxygen required for combusting fuel, and supply all of the heat required from the system. Broadly speaking, two cases arise: (A) operation with the steam cycle able to operate with an unmodified high-pressure and

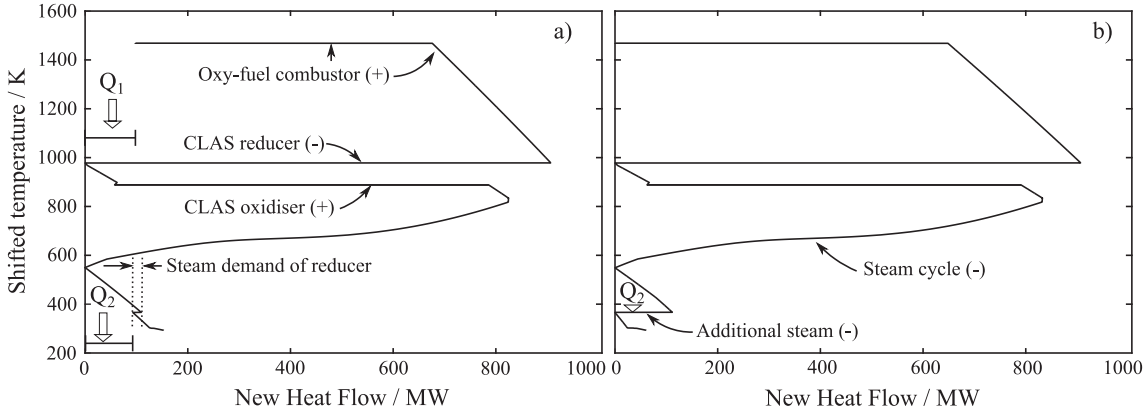

Fig. 3. Grand composite curve of the (a) non-optimized and (b) optimized power plant producing 500 $MW_{el,net}$ running at a heat deficit (Q_1, the part of the heat demand of the CLAS reducer that cannot be satisfied by the oxy-fuel combustor) and using an oxygen carrier system with T_{eq} ($P_{O_2,red}$ = 0.34 bar) = 973 K and ΔH_r^o = 250 kJ/mol; here, the maximum temperature of the unmodified steam cycle is 835 K. Q_1 in (b) is assumed to be overcome by supplying additional oxygen. Q_2 is heat available at temperatures below the steam generator (HRSG) inlet temperature of 549 K. (−) and (+) denote heat sinks and heat sources, respectively.

intermediate-pressure turbine; (B) operation with reduced efficiencies owing to modifications to the high-pressure and intermediate-pressure section of the steam cycle.

3.2.1. Case 2A

In terms of the grand composite curve, case 2A is similar to the optimized case 1, but with all the heat demands of the CLAS system being met by the heat release from combustion. All the heat from CLAS system can be utilized by the steam cycle. CLAS oxygen carrier materials which give composite curves of this kind are desirable.

3.2.2. Case 2B

Case 2B only occurs for oxygen carriers with an equilibrium temperature, $T_{eq}(P_{O_2,ox})$, below the maximum temperature of the base steam cycle, 835 K. In this case, the composite curve of the steam cycle would influence the pinch point at the operating temperature of the CLAS unit. To continue to generate 500 MW electricity, more steam must be produced to make up for the removal of the high temperature turbine segments. In this model, the operating temperature of the steam cycle is kept below that of the oxidizing reactor. In theory, a small amount of heat is still available above the base-case maximum turbine temperature, but to harness it, the steam cycle would have to be reconfigured to utilize the small steam flow which could be produced (heat available between the operating temperatures of the reducer and oxidizer, as shown in Fig. 3); *i.e.* effectively there would have to be either an additional high-pressure turbine or turbine section to process this flow, which is likely to be expensive.

4. Results and discussion

4.1. Variable entropy of reaction

The parameter sweep $\{\Delta H_r^o, T_{eq}\}$ described above allows for a variable entropy of reaction. The result of the parameter sweep is plotted in Fig. 4, when operating the reducing reactor of the CLAS unit at an equilibrium partial pressure of oxygen of 0.34 bar and using Illinois No. 5 coal. Plots for the Hambach lignite and Taldinskaya coal are found in the supplementary information (Figs. S2 and S3). The area for "potential oxygen carriers" shows combinations of ΔH_r^o and T_{eq} likely to be accessible by existing materials; this region is computed by considering the base case (*i.e.* using the thermodynamic assumptions made previously, and the law of Dulong-Petit with $\Delta S^o_{r,298\,K} \equiv S^o_{O_2,298\,K} = 205.2$ J/K/mol) as shown, with the limits set by potential differences in the value of $\Delta S^o_{r,298\,K}$. Here it is assumed that $\Delta S^o_{r,298\,K}$ can differ from the base case by ±25% (although as noted below, some materials could fall outside this bound). The solid iso-lines, showing contours of constant efficiency, indicate that the overall net efficiency of the power plant reaches a plateau at around 40.6% for case 2A. For this case, there is little energy penalty and the overall efficiency is dominated by that of the underlying steam cycle. A vertical boundary separates case 2B and case 2A at 925 K, the temperature at which the operating temperature of the oxidizer forces the maximum temperature of the steam cycle to decrease.

In Fig. 4, the region labelled case 1 corresponds to the situation where the CLAS system cannot be driven by the oxy-fuel combustor as described previously. To operate with these materials would require either heat to be supplied from elsewhere, or extra oxygen to be provided to allow the oxy-fuel combustor to be scaled up to supply the heat demand of the CLAS unit.

From Fig. 4, it is obvious that whether or not the oxy-fuel combustor delivers enough heat is a function of the enthalpy of reaction and the operating temperature of the reducer. With an increase in the temperature at which the oxygen carrier releases oxygen at a specified partial pressure, here 0.34 bar, the maximum feasible enthalpy of reaction, ΔH_r^o, decreases. The gradient of this transition line and its location are a function of the lower heating value of the fuel per mole of oxygen required to combust the fuel. Hence, oxygen carrier systems close to the transition from case 1 to cases 2A and 2B might be feasible when using a fuel with a higher heat of combustion per mole of oxygen required.

4.2. Fixed entropy of reaction

Lines of constant entropy of reaction are shown in Fig. 4 (*e.g.* the base case as illustrated), for a constant temperature difference between the reactors. If, instead, the entropy of reaction is fixed (and the

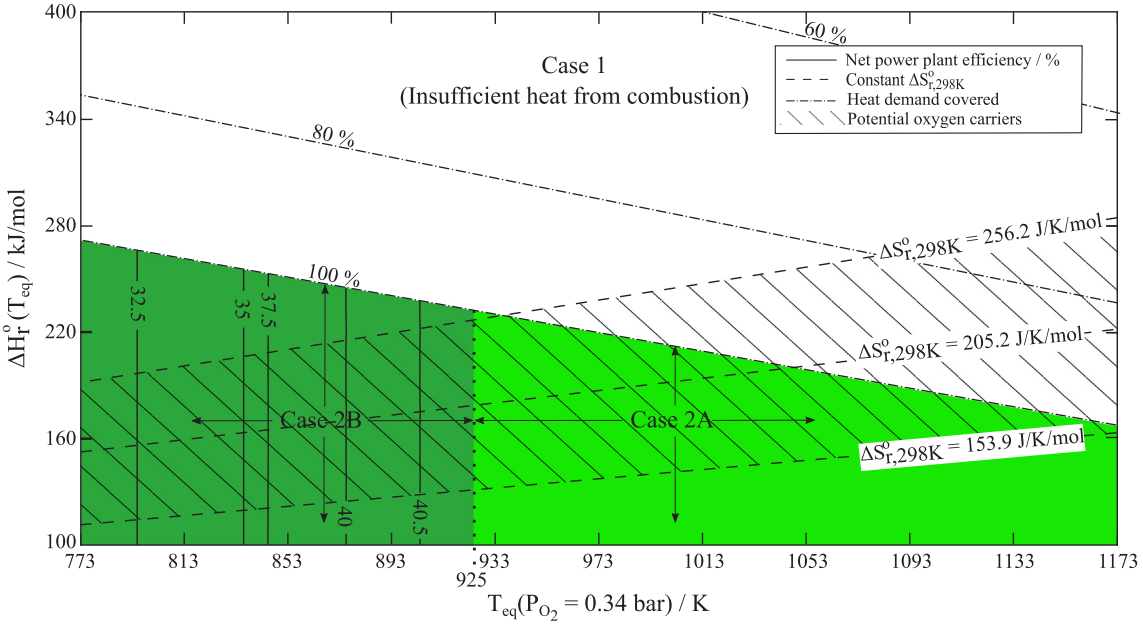

Fig. 4. Efficiency of the CLAS-oxy-fuel power plant depending on thermodynamic properties of the oxygen carrier at an equilibrium partial pressure of oxygen of 0.34 bar in the reducer for the reaction stoichiometry $4XO \rightleftarrows 2X_2\,O + O_2$. The dash-dotted lines show the proportion of the heat demand of the CLAS unit which could be met by a hypothetical oxy-fuel combustor using only the oxygen from the CLAS unit. The temperature difference between the oxidizer and reducer is 80 K. The green region denotes the case where enough heat is supplied from the combustion of fuel. (For interpretation of the references to colour in this figure legend, the reader is referred to the web version of this article.)

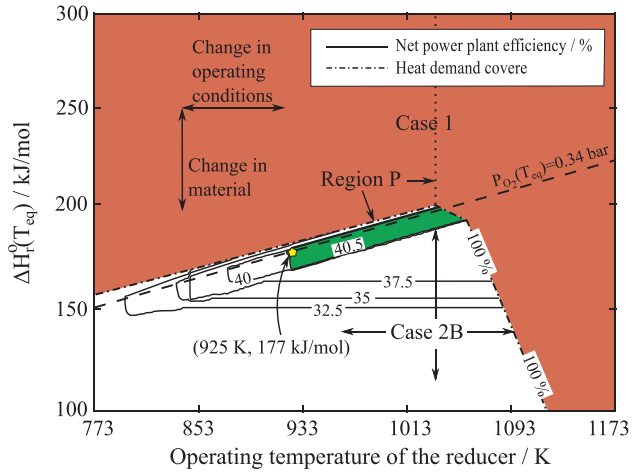

Fig. 5. Efficiency of the CLAS-oxy-fuel power plant depending on thermodynamic properties of the oxygen carrier at a fixed entropy of reaction, $\Delta S_r^o(298\ \mathrm{K}) = 205.2$ J/K/mol. Along the dashed line (which indicates an equilibrium partial pressure of oxygen of 0.34 bar in the reducer), the star marks the transition from case 2B to case 2A, where the efficiency of the plant plateaus at 40.5%. In region P the reducer operates at very low oxygen partial pressures. The red region represents case 1. The green region represents case 2A. (For interpretation of the references to colour in this figure legend, the reader is referred to the web version of this article.)

temperature difference is allowed to vary), the operating space can be replotted. Fig. 5 shows such a plot, with the entropy of reaction fixed to $\Delta S^o_{r,298\ \mathrm{K}} = 205.2$ J/K/mol. Region P in Fig. 5 shows cases where the reducer is operated at very low oxygen partial pressure and, therefore, requires substantial amounts of steam (which is separated out in the CLAS condenser), to meet the requirement of $P_{O_2,req} \cong 0.35$ bar. This high demand for additional steam leads to a significant decrease in the overall net efficiency of the power plant. The dash-dotted line indicates the point at which the oxy-fuel combustor cannot satisfy the heat demand of the CLAS unit, *viz.* transition to case 1 occurs.

Moving horizontally along a line in Fig. 5, the temperature difference between the oxidizer and the reducer can initially be maintained at 80 K to allow $P_{ox} < 0.21$ bar. However, if the reducing reactor is operated above a critical temperature, the difference in temperature between the oxidizer and reducer must be increased to allow the oxidizer to operate with $T_{ox} \rightarrow T_{eq}(P_{O_2} = 0.21\ \mathrm{bar})$.

The transition between case 2A (*i.e.* minimal energy penalty, shaded green) and case 2B in Fig. 5 now occurs for two reasons: (1) vertically at an enthalpy of reaction of around 177 kJ/mol and $T_{eq}(P_{O_2,red} = 0.34\ \mathrm{bar})$ of 925 K, where the oxidizer operates at a temperature of which impacts the steam cycle; (2) along a line parallel to the dashed line, where as the temperature of the reducer increases the air flow to the oxidizer rises as $T_{ox} \rightarrow T_{eq}(P_{O_2} = 0.21\ \mathrm{bar})$, leading to a higher demand in heat to heat up the air that can only be partially recovered into the generation of steam, leading to more heat energy rejected unused and reducing the overall efficiency.

Fig. 6 shows the net efficiency of the base case, *i.e.* $\Delta S^o_{r,298\ \mathrm{K}} = 205.2$ J/K/mol. Here, the CLAS reactors were operated with a difference in temperature of 80 K, where $T_{eq}(P_{O_2,red} = 0.34\ \mathrm{bar})$ is the operating temperature of the reducer. When evaluating oxygen carrier materials for which the assumption of $\Delta S^o_{r,298\ \mathrm{K}} = S^o_{O_2,298\ K}$ holds, the efficiency of the power plant is maximized when $177\ \mathrm{kJ/mol} < \Delta H_r^o(T_{eq}) < 201\ \mathrm{kJ/mol}$.

4.3. Sensitivity to temperature difference of the oxidizer and $T_{eq}(P_{O_2} = 0.21\ \mathrm{bar})$

The difference between the temperature of the oxidizer and the equilibrium temperature for a partial pressure of oxygen of 0.21 bar plays a significant role in the heat integration. The closer the temperature of the oxidizer to $T_{eq}(P_{O_2} = P_{O_2,air} = 0.21\ \mathrm{bar})$, the more air must be supplied to oxidize the reduced oxygen carrier. In the model, the air flow is set to the limiting minimum air flow that allows the oxygen carrier to be fully oxidized, *i.e.* when the depleted air flow has a partial pressure of oxygen, $P_{O_2,ox}$, equal to the equilibrium partial pressure of oxygen of the material at the oxidizer temperature, *i.e.* $P_{O_2,ox} = P_{O_2}(T_{ox})$.

The molar flow of oxygen entering the oxidizer is given by

$$\dot{N}_{O_2,ox,in} = \frac{\dot{N}_{O_2,red}(1-P_{O_2,ox})}{1-\frac{P_{O_2,ox}}{P_{O_2,air}}} \tag{15}$$

where $\dot{N}_{O_2,red}$ is the molar flow of oxygen leaving the reducer, *i.e.* the amount of oxygen required to combust one mole of fuel, and $P_{O_2,ox}$ the equilibrium partial pressure of oxygen at the operating temperature of the oxidizer. When $P_{O_2,ox}$ approaches $P_{O_2,air}$, *i.e.* when $T_{ox} \rightarrow T_{eq}(P_{O_2} = 0.21\ \mathrm{bar})$, the air flow must increase, and in the limiting case of $T_{ox} = T_{eq}(P_{O_2} = 0.21\ \mathrm{bar})$ is infinite. Fig. 7 shows both the net efficiency of the power plant and the air flow as a function of the operating temperature of the oxidizer for three materials with the same T_{eq} ($P_{O_2,red} = 0.34$ bar), different enthalpies of reaction, and, hence, varying entropies of reaction. For a given T_{eq} ($P_{O_2,red} = 0.34$ bar) the gradient of the equilibrium curve increases for materials with higher enthalpies of reaction and the oxidizer can be operated at a temperature closer to that of the reducer.

4.4. Support material and partial conversion

If either a support material is used or there is only partial conversion of the oxygen carrier, solid material is circulated that does not participate in the redox reaction. This inert material circulates heat between the colder oxidizer and the hotter reducer. Hence, the addition of inert support material, here α-Al_2O_3 or β-SiO_2, decreases the combinations of ΔH_r^o and T_{eq} at which autothermal operation is possible. In Fig. 8, these combinations are plotted for molar fractions of inert material of 0%, 50% and 75% and autothermal operation can be achieved below the respective lines. Similar to the addition of inert material, the heat load of the reactors changes if partial conversion is assumed or the flue gas recirculation rate is increased, *i.e.* lowering the operating partial pressure of oxygen in the reducer; results for the latter are plotted Fig. S1 in the supplementary information.

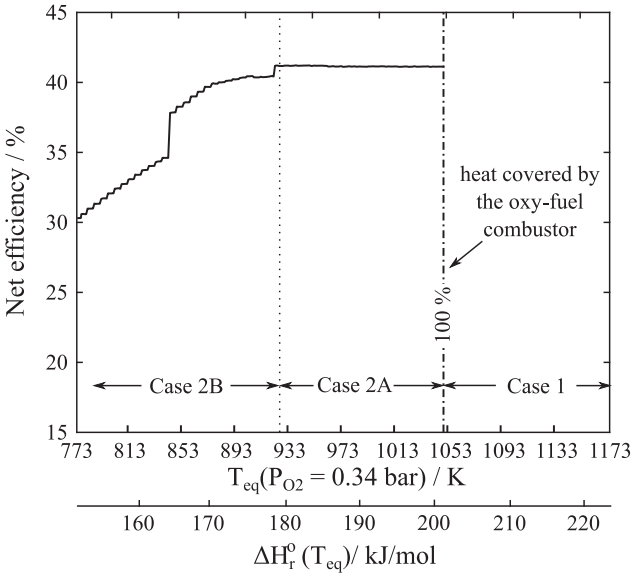

Fig. 6. Net efficiency of the power plant vs oxygen carrier materials with an entropy of reaction of 205.2 J/K/mol, an equilibrium partial pressure of oxygen of 0.34 bar in the reducer a reaction. a stoichiometry of $4XO \rightleftarrows 2X_2\ O + O_2$ and difference in the operating temperatures of the CLAS reactors of 80 K.

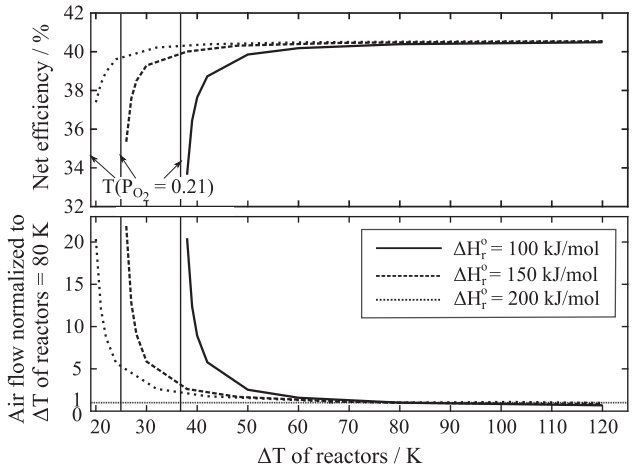

Fig. 7. Sensitivity of the net efficiency of the CLAS oxy-fuel power plant and the normalized air flow to the oxidizer with respect to the temperature difference between oxidizer and reducer and three oxygen carriers. Here, the reducer is operated at 973 K.

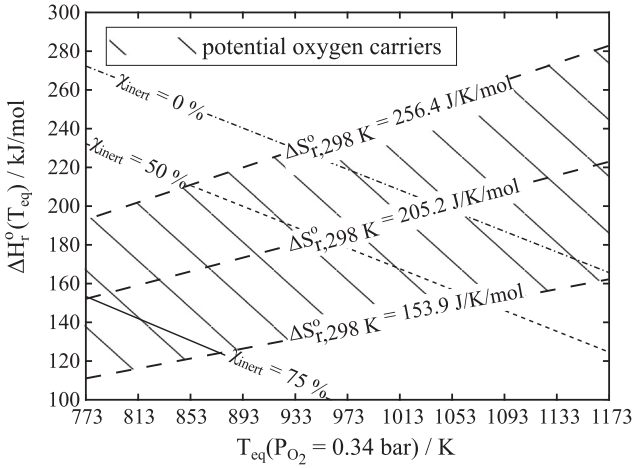

Fig. 8. Suitable regions for autothermal operation using 0 mol-%, 50 mol-% or 75 mol-% of α-Al_2O_3 below the respective lines using fictitious oxygen carriers following the reaction 4XO ⇄ 2X_2 O+ O_2 and Illinois No. 5 coal.

4.5. Effect of specific heat capacity of the solids

Previously, it was assumed that the law of Dulong-Petit holds to obtain the molar heat capacity, C_p, for the solids. This is likely to lead to little error in terms of the equilibrium calculation, because only the difference in molar heat capacity of reaction, $\Delta C_{p,r}$, is important. However, from the point of view of heat integration, the absolute value of C_p is important, because the solids transport sensible heat between the colder oxidizer and the hotter reducer. All the previous calculations have assumed absolute values for the molar heat capacity of the reduced, $C_{p,red}$, and oxidized phase, $C_{p,ox}$, derived from the atoms and stoichiometry, which gives a $\Delta C_{p,r}$ that is only a function stoichiometric coefficient of oxygen. Fig. S4 in the supplementary information shows the efficiency of the CLAS-oxy-fuel power plant with a different reaction stoichiometry (6$X_{4/3}$ O⇄ 4X_2 O+ O_2) than the previously assumed, *i.e.* 4XO ⇄ 2X_2 O+ O_2. The range of $\{\Delta H_r^o, T_{eq}\}$ decreased due to higher molar heat capacities. Hence, the sensitivity of the previous calculations would be the same as that described above, *i.e.* any increase in absolute C_p would have the same effect as adding inert material or partially converting the solid.

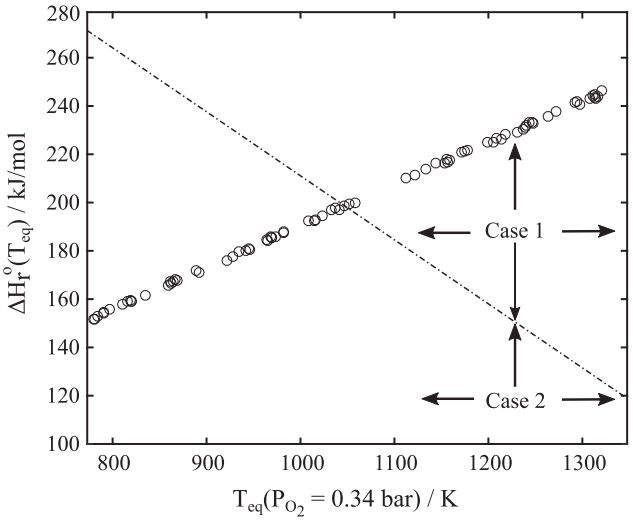

Fig. 9. Enthalpy of reaction and equilibrium temperature of 79 shortlisted oxygen carrier systems for 673 K⩽ T_{eq} ⩽ 1323 K based on dft calculations; the dash-dotted line denotes the transition between autothermal (case 2) and endothermic operation (case 1) when using Illinois No. 5 coal (as in Fig. 4).

4.6. Screening of materials based on DFT

A full list of the 2857 candidates screened from the Materials Project data base is given in Table S3 in the supplementary information. Of these, only 79 had equilibrium operating temperatures in the range 673–1323 K (a slightly wider temperature range than that used previously to allow for errors in the DFT) and a bimolecular oxidation reaction only. These candidate materials, the thermodynamic data of which were derived from density functional theory (DFT), are shown on the plot of $\Delta H_r^o(T_{eq})$ *vs.* $T_{eq}(P_{O_2,red} = 0.34)$ in Fig. 9 (the complete list of the 79 oxygen carriers is provided in Table S2 in the supplementary information). The figure shows the boundary between cases 1 and 2 for the case where Illinois No. 5 coal is used, and the molar heat capacities are set in accordance with the law of Dulong-Petit. The position of this line therefore can vary slightly depending on fuel and stoichiometry of the oxygen release reaction as discussed previously. Of the candidate materials, 34 were found to achieve autothermal operation, but, since there are both errors in the DFT and the boundary for autothermal operation can move, oxygen carrier materials not in Table 1 might work, too.

In Table 1, toxicity and cost have been neglected. The main criterion was that only one phase transition occurs at the temperatures of interest. It should be noted that Table 1 has to be treated with caution; for some materials, their suitability as an oxygen carrier has been questioned. For example, BaO_2, the material used in the Brin process, is vulnerable to carbonation [6]. For BaO_2, at a partial pressure of oxygen of 0.34 bar, the predicted equilibrium temperature of around 784 K is in reasonable agreement with an equilibrium temperature of around 865 K observed experimentally [39]. However, using the DFT calculated equilibrium temperature of 784 K would lead to an efficiency as low as 31.5%, according to the model underlying this study. If instead, the experimentally-determined value of $T_{eq}(P_{O_2,red} = 0.34\ \text{bar}) = 865$ K were used, from Fig. 4, the efficiency would be ~39%. This again highlights that materials operating in non-desirable regions, *viz.* case 2B, might still be worth investigating. Commentary on oxygen carriers identified to fall into case 2A but are not feasible, *e.g.* due to their melting point, is provided in the supplementary information.

Finally, considering melting points, thermodynamic stability and health hazards, the suggested list of potentially suitable oxygen carriers in Table 1 reduces to $BaFeO_3/Ba_2Fe_2O_5$, $LiBiO_3/LiBiO_2$, $MnPO_4/Mn_2P_2O_7$, $SrFeO_3/Sr_2Fe_2O_5$, and $Sr_2Cu_2O_5/SrCuO_2$. The perovskite $BaFeO_{2.93}$ was found to decompose into the brownmillerite phase

Table 1
Promising oxygen carrier systems deduced from DFT calculations. OC = oxygen carrier.

Oxidized OC	Reduced OC	$T_{eq}(P_{O2,red} = 0.34)$ (K)	$\Delta H_r^o(T_{eq})$ (kJ/mol)	Net efficiency	Case
$CoSeO_4$	$CoSeO_3$	928	178	40.6%	2A
CsO_2	$Cs_{11}O_3$	1041	197	40.6%	2A
CsO_2	Cs_3O	942	180	40.6%	2A
$CsIO_4$	CsI	946	181	40.6%	2A
$Hg(IO_3)_2$	HgI_2	1015	193	40.6%	2A
$KAgO_2$	KAgO	965	184	40.6%	2A
$KBiO_3$	$KBiO_2$	945	181	40.6%	2A
$MnSeO_4$	$MnSeO_3$	970	185	40.6%	2A
$NaMnO_4$	$Na_2Mn_2O_3$	982	188	40.6%	2A
$NaBiO_3$	$NaBiO_2$	1009	192	40.6%	2A
PbO_2	PbO	935	180	40.6%	2A
$Sm_2Mn_2O_7$	$SmMnO_3$	979	188	40.6%	2A
$Tl(IO_3)_3$	TlI_3	1037	198	40.6%	2A
$V_2Hg_2O_7$	$VHgO_3$	1030	197	40.6%	2A
Ag_2SeO_4	Ag_2SeO_3	892	171	40.4%	2B
$BaFeO_3$	$Ba_2Fe_2O_5$	922	176	40.6%	2B
BaO_2	BaO	781	152	31.5%	2B
$CdSeO_4$	$CdSeO_3$	780	152	31.4%	2B
Eu_3ReO_8	Eu_3ReO_7	860	166	39.3%	2B
Hg_2SeO_5	Hg_2SeO_3	862	166	39.4%	2B
$Ho_2(SeO_4)_3$	$Ho2(SeO_3)_3$	835	162	35.0%	2B
$LiBiO_3$	$LiBiO_2$	784	153	31.7%	2B
$MnPO_4$	$Mn_2P_2O_7$	820	159	34.1%	2B
MnO_2	Mn_3O_4	869	168	39.8%	2B
$Mn(SeO_3)_2$	$MnSe_2O_5$	791	154	32.2%	2B
$NaAgO_2$	NaAgO	865	167	39.6%	2B
$Na_2Cr_2O_7$	$NaCrO_2$	811	158	33.6%	2B
RbO_3	Rb_2O_3	819	159	34.0%	2B
$SbOF_3$	SbF_3	889	172	40.4%	2B
$SrFeO_3$	$Sr_2Fe_2O_5$	816	159	33.9%	2B
$SrCr_2O_7$	$SrCr_2O_4$	791	155	32.2%	2B
$Sr_2Cu_2O_5$	$SrCuO_2$	797	156	32.6%	2B
Ti_2O_7	Ti_3O_5	867	168	39.7%	2B
V_2O_5	V_3O_7	861	167	39.4%	2B

$Ba_2Fe_2O_5$ giving off oxygen equal to 2.9% of its mass at around 1073 K [40]. Here, the error in the DFT-derived equilibrium temperature becomes apparent; under the assumptions used in the model, decomposition to $Ba_2Fe_2O_5$ was expected at 901 K at an oxygen partial pressure of 0.21 bar. Whilst the reduction of the perovskite phase is possible, it was found that oxidation of $Ba_2Fe_2O_5$, *i.e.* cooling in air, did not proceed [40]. For $LiBiO_3$, the release of oxygen was reported at temperatures above 573 K [41]. Full reduction to $LiBiO_2$ was achieved at around 773 K [41,42], re-oxidation, however, was not evaluated. $SrFeO_3$ was found to cycle between the perovskite phase and the brownmillerite phase, Sr_2Fe_2O5, reversibly for at least two cycles at 973 K [22], and for at least 20 cycles at 823 K without showing susceptibility towards carbonation when reduced in CO_2 [43]. $Sr_2Cu_2O_5$ was synthesized at 1123 K and 100 kbar using $SrCuO_2$ as a precursor [44], conditions beyond those expected in chemical looping systems. However, $SrCuO_2$ was used as an oxygen carrier in chemical looping combustion, releasing oxygen equal to around 8% of its mass at 873 K to form $SrCuO_{1.075}$ [45]. This oxygen carrier system exhibited further stability over 20 redox cycles at 1223 K.

4.7. Commonly-cited materials for CLAS

When looking at established oxygen carrier systems, *i.e.* CuO/Cu_2O, Mn_2O_3/Mn_3O_4 and CoO/Co_3O_4, the respective combinations of thermodynamic properties fall well within case 1, *viz.* endothermic operation. However, the previous results in this paper did not allow for any heat recovery in the form of preheating of the recycled flue gas to the reducer or gaseous inflow to the oxy-fuel combustor. Both these can alter the boundary for autothermal operation, though it should be noted that the compressor and fans used in recycle systems would limit the degree of possible preheating. Fig. 10 shows that for CuO/Cu_2O, Mn_2O_3/Mn_3O_4 and CoO/Co_3O_4, the requirement for additional oxygen or heat is significant, particularly if there is no preheating of the recycled flue gas or the incoming air. Among the fuels discussed here, the Illinois No. 5 coal achieves the least deficit in heat (Q_1 in Fig. 3); using Illinois No. 5 coal with Mn_2O_3/Mn_3O_4 and preheating the CO_2 stream to the reducing reactor and gaseous inflow to the oxy-fuel combustor to 673 K and 573 K, respectively, allows for 95.6% of the heat demand of the reducing reactor to be met by the heat released in the oxy-fuel

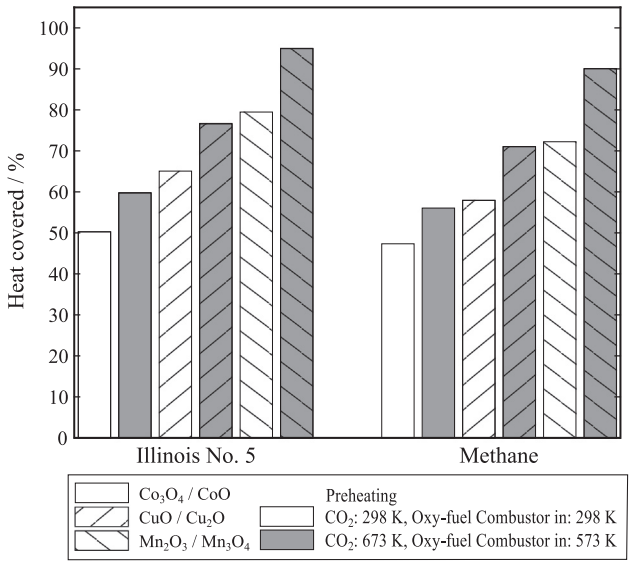

Fig. 10. Amount of heat demand of the reducer covered by the combustion of Illinios No. 5 coal or methane for CuO/Cu_2O, Mn_2O_3/Mn_3O_4 and CoO/Co_3O_4 and different preheating temperatures for CO_2 to the reducer and gas flow to the oxy-fuel combustor.

combustor. These temperatures were chosen in accordance with the maximum operation temperature of radial fans of 723 K for the scales required, and favourable temperatures for gas entering the oxy-fuel combustor of 473–673 K, respectively [46]. The ability of Hambach lignite and methane to cover the heat demanded by the respective oxygen carrier is similar, owing to their almost identical molar LHV per mole of oxygen required for combustion, despite significant differences in the LHVs (11.3 MJ/kg and 49.9 MJ/kg, respectively). The LHV per mole of oxygen of both Taldinskaya coal and Hambach lignite are lower than that of Illinois No. 5 coal and therefore neglected here.

Furthermore, the results provided in Fig. 10 assume no doping with support material. In practice, however, these materials require the addition of support material owing to either their inability to reoxidize without support material, such as Mn_2O_3/Mn_3O_4 [47], or the desired mechanical strength and resistance against sintering [15,48–50].

It should be noted that the combination of the equilibrium temperature, $T_{eq}(P_{O_2,red} = 0.34)$, and enthalpy of reaction, $\Delta H^o_{r,298\,K}$, of the Cobalt oxide, as shown in Table 2, is outside of the region of potential oxygen carriers of Fig. 4. The reason is the significant deviation in the entropy of reaction from the assumed entropy of reaction, $\Delta S^o_{r,298\,K}$, of 205.2 J/K/mol, *i.e.* outside the ± 25% shown in Fig. 4.

4.8. Limitations

There are a number of limitations to the methods used in this study. The assessment of oxygen carriers of which only the enthalpy of reaction is known, as is the case with oxygen carrier systems deduced from the Materials Project [34], might give inaccurate results due to a significant deviation of the entropy of reaction from the assumed value, as described above.

Secondly, the integration of heat with the steam cycle takes a fairly basic approach, leading to case 2B when the operating temperature of the oxidizer falls below 845 K (assuming a ΔT_{min} of heat exchange of 10 K). For example, instead of lowering the maximum temperature of the steam cycle, an additional high-pressure turbine could be employed to operate at temperatures above the reducer if the oxygen carrier were able to release oxygen at low enough temperatures, as mentioned previously. Entirely different designs of the oxy-fuel power plant are conceivable as well, such as a combined cycle, provided the enthalpy of reaction of the oxygen carrier is small compared to the lower heating value per mole of oxygen of the fuel. Here, a gas turbine could generate electricity at temperatures above the operating temperature of the reducer and supply heat to the reducer. The oxidizer would then be the major source of heat for the steam cycle.

Another major limitation to the approach taken here to identify suitable oxygen carriers of CLAS is the neglect of the reaction kinetics. Candidate materials that seem suitable for CLAS might in fact react slowly, a typical example being the oxidation of Mn_3O_4 to Mn_2O_3 which was reported to be unachievable at 1173 K [47,51,52], even though it is thermodynamically feasible.

From the study of heat integration performed in this paper, it is obvious that employing a temperature swing between the reducer and oxidizer to separate air is not ideal. If, instead, pressure swing could be used, the temperature at which the transition between cases 2A and 2B occurs would decrease. Therefore, oxygen carriers releasing oxygen at temperatures above the maximum temperature of the steam cycle would fall into case 2A, *i.e.* autothermal operation with very little energy penalty.

Table 2
Model input, T_{eq} and ΔH_r, and output for CuO/Cu_2O, Mn_2O_3/Mn_3O_4 and CoO/Co_3O_4.

Oxygen carrier	T_{eq} ($P_{O_2,red}$ = 0.34bar) (K)	$\Delta H^o_{r,298\,K}$ (kJ/mol)	$\Delta S^o_{r,298\,K}$ (J/K/mol)
CuO/Cu_2O [27]	1324	281.1	219.4
Mn_2O_3/Mn_3O_4 [32]	1179	195.0	158.3
Co_3O_4/CoO [31]	1185	393.6	293.4

5. Conclusions

A model was constructed which links the thermodynamic properties of an oxygen carrier to the steady state operation of an oxy-fuel power plant to estimate the viability of oxygen carriers for chemical looping air separation. This methodology allows the impact on the process of material properties, *i.e.* enthalpy ($\Delta H^o_{r,298\,K}$) and entropy ($\Delta S^o_{r,298\,K}$) of reaction, to be rationally assessed. The CLAS-oxy-fuel process can be characterized fully by a 2D map in which performance is a function of either $\Delta H^o_{r,298\,K}$ and $\Delta S^o_{r,298\,K}$ or, as presented here, as a function of the temperature at which the material is in equilibrium with 0.34 mol.% O_2 (T_{eq}), and the heat of reaction at T_{eq}, $\Delta H^o_r(T_{eq})$.

Superimposing (1) measured data from known materials, (2) prospective materials with properties drawn from the Materials Project database of theoretical DFT calculations, and (3) hypothetical materials allows the following conclusions to be drawn:

1. Lower values of T_{eq} of the oxygen carrier material widen the range of acceptable values of $\Delta H^o_r(T_{eq})$ for autothermal operation, *i.e.* when there is sufficient heat from the oxy-fuel combustion to support the metal oxide reduction.
2. The range of $\Delta H^o_r(T_{eq})$ and T_{eq} which allow for autothermal operation (as opposed to requiring additional heat from external sources) increases with the molar lower heating value per mole of oxygen required by the fuel, θ, and the degree of preheating. More heat being available from the combustion of fuel allows for more endothermic reactions in the reducer, *i.e.* higher ΔH^o_r.
3. Using the investigated fuels, *viz.* Hambach lignite (θ = 380 kJ/mol O_2), Illinois No. 5 coal (θ = 396 kJ/mol O_2) and Taldinskaya coal (θ = 372 kJ/mol O_2), commonly-cited oxygen carriers CuO/Cu_2O, CoO/Co_3O_4 and Mn_2O_3/Mn_3O_4 do not allow for autothermal operation; even without the addition of support materials α-Al_2O_3 or β-SiO_2. Here, both the gaseous inflow to the oxy-fuel combustor and the carbon dioxide stream to the reducer were preheated to 573 K and 673 K, respectively.
4. Operating the oxidizing reactor at temperatures below the maximum steam temperature of the unmodified steam cycle (here 835 K) leads to reduced net efficiencies, and requires the steam cycle to be operated with a lower turbine inlet temperature.
5. Having identified suitable combinations of ΔH^o_r and T_{eq}, 34 oxygen carrier systems allowing for an autothermal operation of the CLAS-oxy-fuel power plant have been suggested, based on DFT calculations. Of these, five systems seem particularly promising, namely $BaFeO_3/Ba_2Fe_2O_5$, $LiBiO_3/LiBiO_2$, $MnPO_4/Mn_2P_2O_7$, $SrFeO_3/Sr_2Fe_2O_5$, and $Sr_2Cu_2O_5/SrCuO_2$.

These results show that a parameter sweep of thermodynamic properties using a macro-model of a power plant is an efficient approach to identify novel oxygen carrier candidates, when tied to density functional theory.

Acknowledgements

M.T. Dunstan is supported by a Junior Research Fellowship from Clare College, Cambridge, and a STFC Early Career Award. W. Hu, M. T. Dunstan, S. A. Scott and J. S. Dennis acknowledge funding from EPSRC Grant No. EP/K030132/1.

Data access

All supporting data will be available https://www.repository.cam.ac.uk/.

Appendix A. Supplementary material

Supplementary data associated with this article can be found, in the online version, at http://dx.doi.org/10.1016/j.apenergy.2017.11.083.

References

[1] McCauley K, Moorman S, McDonald D. Oxy-coal combustion for low carbon electric power generation. Spain: Zaragoza; 2011.

[2] Shah K, Moghtaderi B, Zanganeh J, Wall T. Integration options for novel chemical looping air separation (ICLAS) process for oxygen production in oxy-fuel coal fired power plants. Fuel 2013;107:356–70. http://dx.doi.org/10.1016/j.fuel.2013.01.007.

[3] Pfaff I, Kather A. Comparative thermodynamic analysis and integration issues of CCS steam power plants based on oxy-combustion with cryogenic or membrane based air separation. Energy Proc 2009;1:495–502. http://dx.doi.org/10.1016/j.egypro.2009.01.066.

[4] Kanniche M, Gros-Bonnivard R, Jaud P, Valle-Marcos J, Amann JM, Bouallou C. Pre-combustion, post-combustion and oxy-combustion in thermal power plant for CO_2 capture. Appl Therm Eng 2010;30:53–62. http://dx.doi.org/10.1016/j.applthermaleng.2009.05.005.

[5] Fu C, Gundersen T. Exergy analysis and heat integration of a coal-based oxy-combustion power plant. Energy Fuels 2013;27:7138–49. http://dx.doi.org/10.1021/ef400867d.

[6] Jensen WB. Ask the historian the origin of the brin process for the manufacture of oxygen. J Chem Educ 2009;86:1266–7.

[7] Y.-S. Lin, D.L. MacLean, Y. Zeng, High temperature adsorption process, US Patent no: 6059858; 2000.

[8] Yang Z, Lin YS, Zeng Y. High-temperature sorption process for air separation and oxygen removal. Ind Eng Chem Res 2002;41:2775–84. http://dx.doi.org/10.1021/ie010736k.

[9] Li Z, Zhang T, Cai N. Experimental study of O_2 - CO_2 production for the oxyfuel combustion using a co-based oxygen carrier. Ind Eng Chem Res 2008;47:7147–53.

[10] Moghtaderi B. Application of chemical looping concept for air separation at high temperatures. Energy Fuels 2010;24:190–8. http://dx.doi.org/10.1021/ef900553j.

[11] Wall T, Liu Y, Spero C, Elliott L, Khare S, Rathnam R, et al. An overview on oxyfuel coal combustion-state of the art research and technology development. Chem Eng Res Des 2009;87:1003–16. http://dx.doi.org/10.1016/j.cherd.2009.02.005.

[12] T. Wall, Fundamentals of oxy-fuel combustion. In: Oxy-fuel combust. Res. Netw., Cottbus, Germany; 2005.

[13] Buhre BJP, Elliott LK, Sheng CD, Gupta RP, Wall TF. Oxy-fuel combustion technology for coal-fired power generation. Prog Energy Combust Sci 2005;31:283–307. http://dx.doi.org/10.1016/j.pecs.2005.07.001.

[14] Adanez J, de Diego LF, Garcıa-Labiano F, Gayan P, Abad A, Palacios JM. Selection of oxygen carriers for chemical-looping combustion. Energy Fuels 2004;18:371–7.

[15] Chuang SY, Dennis JS, Hayhurst AN, Scott SA. Development and performance of Cu-based oxygen carriers for chemical-looping combustion. Combust Flame 2008;154:109–21. http://dx.doi.org/10.1016/j.combustflame.2007.10.005.

[16] Adanez J, Abad A, Garcia-Labiano F, Gayan P, de Diego LF. Progress in chemical-looping combustion and reforming technologies. Prog Energy Combust Sci 2012;38:215–82. http://dx.doi.org/10.1016/j.pecs.2011.09.001.

[17] Imtiaz Q, Hosseini D, Rüdiger C. Review of oxygen carriers for chemical looping with oxygen uncoupling (CLOU): thermodynamics. Material Develop Synth Energy Technol 2013;1:633–47. http://dx.doi.org/10.1002/ente.201300099.

[18] Zhang J, He T, Wang Z, Zhu M, Zhang K, Li B, et al. The search of proper oxygen carriers for chemical looping partial oxidation of carbon. Appl Energy 2017;190:1119–25. http://dx.doi.org/10.1016/j.apenergy.2017.01.024.

[19] Siriwardane R, Tian H, Miller D, Richards G. Fluidized bed testing of commercially prepared MgO-promoted hematite and CuO–Fe_2O_3 mixed metal oxide oxygen carriers for methane and coal chemical looping combustion. Appl Energy 2015;157:348–57. http://dx.doi.org/10.1016/j.apenergy.2015.04.042.

[20] Galinsky N, Mishra A, Zhang J, Li F. $Ca_{1-x}A_xMnO_3$ (A = Sr and Ba) perovskite based oxygen carriers for chemical looping with oxygen uncoupling (CLOU). Appl Energy 2015;157:358–67. http://dx.doi.org/10.1016/j.apenergy.2015.04.020.

[21] Ikeda H, Tsuchida A, Morita J, Miura N. $SrCo_xFe_{1-x}O_{3-\delta}$ oxygen sorbent usable for high-temperature pressure-swing adsorption process operating at approximately 300 °C. Ind Eng Chem Res 2016;55:6501–5. http://dx.doi.org/10.1021/acs.iecr.6b01284.

[22] Taylor DD, Schreiber NJ, Levitas BD, Xu W, Whitfield PS, Rodriguez EE. Oxygen storage properties of $La_{1-x}Sr_xFeO_{3-\delta}$ for chemical-looping reactions – an in-situ neutron and synchrotron X-ray study. Chem Mater 2016;28:3951–60. http://dx.doi.org/10.1021/acs.chemmater.6b01274.

[23] Zakutayev A, Zhang X, Nagaraja A, Yu L, Lany S, Mason TO, et al. Theoretical prediction and experimental realization of new stable inorganic materials using the inverse design approach. J Am Chem Soc 2013;135:10048–54. http://dx.doi.org/10.1021/ja311599g.

[24] Zhang X, Yu L, Zakutayev A, Zunger A. Sorting stable versus unstable hypothetical compounds: the case of multi-functional ABX Half-Heusler filled tetrahedral structures. Adv Funct Mater 2012;22:1425–35. http://dx.doi.org/10.1002/adfm.201102546.

[25] Dunstan MT, Jain A, Liu W, Ong SP, Liu T, Lee J, et al. Large scale computational screening and experimental discovery of novel materials for high temperature CO_2 capture. Energy Environ Sci 2016;9:1346–60. http://dx.doi.org/10.1039/C5EE03253A.

[26] Sonntag D. Important new values of the physical constants of 1986, vapour pressure formulations based on the IST-90 and psychrometer formulae. Zeitung Für Meteorol 1990;70:340–4.

[27] McBride BJ, Zehe MJ, Gordon S. NASA Glenn coefficients for calculating thermodynamic properties of individual species, Ohio; 2002. http://hdl.handle.net/2060/20020085330.

[28] Sperlich V. Übungsaufgaben zur Thermodynamik mit Mathcad, Carl Hanser Verlag. Leipzig 2002. http://dx.doi.org/10.3139/9783446222380.

[29] Grote K-H, Feldhusen J. Dubbel — Taschenbuch für den Maschinenbau, 22nd ed. Berlin, Heidelberg: Springer Berlin Heidelberg; 2007 10.1007/978-3-662-06774-1.

[30] Cooper JR, Mary Q, Road ME, Associates SI. Revised release on the IAPWS industrial formulation 1997 for the thermodynamic properties of water and steam; 2012.

[31] Chase MWJ. NIST-JANAF thermochemical tables. New York: American Institute of Physics; 1998.

[32] Barin I, Knacke O. Thermochemical properties of inorganic substances. Springer; 1974.

[33] Ong SP, Wang L, Kang B, Ceder G. $Li-Fe-P-O_2$ phase diagram from first principles calculations. Chem Mater 2008;20:1798–807. http://dx.doi.org/10.1021/cm702327g.

[34] Jain A, Ong SP, Hautier G, Chen W, Richards WD, Dacek S, et al. Commentary: the materials project: a materials genome approach to accelerating materials innovation. APL Mater 2013;1. http://dx.doi.org/10.1063/1.4812323.

[35] Wang L, Maxisch T, Ceder G. Oxidation energies of transition metal oxides within the GGA + U framework. Phys Rev B - Condens Matter Mater Phys 2006;73:1–6. http://dx.doi.org/10.1103/PhysRevB.73.195107.

[36] Ong SP, Jain A, Hautier G, Kang B, Ceder G. Thermal stabilities of delithiated olivine MPO_4 (M = Fe, Mn) cathodes investigated using first principles calculations. Electrochem Commun 2010;12:427–30. http://dx.doi.org/10.1016/j.elecom.2010.01.010.

[37] Dennis JS, Müller CR, Scott SA. In situ gasification and CO2 separation using chemical looping with a Cu-based oxygen carrier: performance with bituminous coals. Fuel 2010;89:2353–64. http://dx.doi.org/10.1016/j.fuel.2010.01.037.

[38] Trainer JP, Perrin N, Darde A. Update on advanced developments for ASU and CO_2 purification units for oxy-combustion (Air Liquide, France). In: 3rd Meet. Oxy-Combustion Netw., Yokohama, Japan, March 5th; 2008.

[39] Till L. Thermochemical data of barium peroxide from thermogravimetric measurements. J Therm Anal 1971;3:177–80. http://dx.doi.org/10.1007/BF01904681.

[40] Parras M, González-Calbet JM, Vallet-Regí M, Grenier JC. A high temperature study of the $BaFeO_{3-y}$ system. Solid State Ionics 1993;63–65:714–8. http://dx.doi.org/10.1016/0167-2738(93)90185-6.

[41] Kumada N. Preparation and crystal structure of a new lithium bismuth oxide: $LiBiO_3$. J Solid State Chem 1996;126:121–6. http://dx.doi.org/10.1006/jssc.1996.0319.

[42] Sathiyamoorthi R, Subramania A, Gangadharan R, Vasudevan T. Preparation of nanoparticle size $LiBiO_2$ by combustion method and its electrochemical studies for lithium secondary cells. Pramana - J Phys 2005;65:973–80. http://dx.doi.org/10.1007/BF02704099.

[43] Lau CY, Dunstan MT, Hu W, Grey CP, Scott SA. Large scale in silico screening of materials for carbon capture through chemical looping. Energy Environ Sci 2017;10:818–31. http://dx.doi.org/10.1039/C6EE02763F.

[44] Chen BH, Walker D, Scott BA, Mitzi DB. Synthesis and structure of a new perovskite, $SrCuO_{2.5}$. J Solid State Chem 1996;121:498–501. http://dx.doi.org/10.1006/jssc.1996.0070.

[45] Ksepko E. Examining $SrCuO_2$ as an oxygen carrier for chemical looping combustion. J Therm Anal Calorim 2015;122:621–33. http://dx.doi.org/10.1007/s10973-015-4813-8.

[46] Kather A, Scheffknecht G. The oxycoal process with cryogenic oxygen supply. Naturwissenschaften 2009;96:993–1010. http://dx.doi.org/10.1007/s00114-009-0557-2.

[47] Shulman A, Cleverstam E, Mattisson T, Lyngfel A. Manganese/iron, manganese/nickel, and manganese/silicon oxides used in chemical-looping with oxygen uncoupling (CLOU) for combustion of methane. Energy Fuels 2009;23:5269–75. http://dx.doi.org/10.1021/ef9005466.

[48] Arjmand M, Azad AM, Leion H, Rydén M, Mattisson T. $CaZrO_3$ and $SrZrO_3$-based CuO oxygen carriers for chemical-looping with oxygen uncoupling (CLOU). Energy Proc 2013;51:75–84. http://dx.doi.org/10.1016/j.egypro.2014.07.009.

[49] Gayán P, Adánez-rubio I, Abad A, De Diego LF, García-labiano F, Adánez J. Development of Cu-based oxygen carriers for Chemical-Looping with Oxygen Uncoupling (CLOU) process. Fuel 96 (2012) 226–238. 10.1016/j.fuel.2012.01.021.

[50] Shah K, Moghtaderi B, Wall T. Selection of suitable oxygen carriers for chemical looping air separation: a thermodynamic approach. Energy Fuels 2012;26:2038–45. http://dx.doi.org/10.1021/ef300132c.

[51] Zafar Q, Abad A, Mattisson T, Gevert B, Strand M. Reduction and oxidation kinetics of Mn_3O_4/Mg-ZrO_2 oxygen carrier particles for chemical-looping combustion. Chem Eng Sci 2007;62:6556–67. http://dx.doi.org/10.1016/j.ces.2007.07.011.

[52] Francis TM, Perkins C, Weimer AW. Manganese oxide dissociation kinetics for the Mn_2O_3 thermochemical water-splitting cycle. Part 2: CFD model. Chem Eng Sci 2010;65:4397–410. http://dx.doi.org/10.1016/j.ces.2010.03.048.